

Quantum phase estimation in presence of glassy disorder

Soubhadra Maiti^{1,2}, Kornikar Sen², Ujjwal Sen²

¹Indian Institute of Science Education and Research, Pune 411 008, India

²Harish-Chandra Research Institute, HBNI, Chhatmag Road, Jhansi, Allahabad 211 019, India

We investigate the response to noise, in the form of glassy disorder present in circuit elements, in the success probability of the quantum phase estimation algorithm, a subroutine used to determine the eigenvalue - a phase - corresponding to an eigenvector of a unitary gate. We consider three types of disorder distributions: Haar-uniform with a circular finite cut-off, Haar-uniform with a squeezed cut-off, and spherical normal. We examine the behavior of the probability of estimating the correct phase in response to the inflicted disorder. There is generally a depreciation of the quenched averaged success probability in response to the disorder incorporation. Even in the presence of the disorder, increasing the number of auxiliary qubits helps to get a better precision of the phase, albeit to a lesser extent than that in the clean case. We find a concave to convex transition in the dependence of probability on the degree of disorder when the distribution at hand is Haar-uniform, and a log-log dependence is witnessed between the strength of disorder at the point of inflection and the number of auxiliary qubits used.

I. INTRODUCTION

There are various aspects of quantum mechanics that make it strikingly distinct from its classical cousin. Harnessing the power of these quantum characteristics provide or are believed to provide significantly improved efficiencies in numerous quantum algorithms with respect to the corresponding classical algorithms [1–3]. Examples include the Deutsch–Jozsa algorithm [4, 5], Shor’s algorithm [6], Grover’s algorithm [7], etc.

The quantum phase estimation algorithm (QPEA) [8–10] is tailored to determine the eigenvalues, which are phases, of a given unitary operator. Quantum phase estimation is applicable to problems that can effectively be turned into solving an eigenvalue equation such as computing molecular spectra [11–13]. Shor’s algorithm for prime factorization of integers, which classically is believed to take a number of steps that is exponential in the input size, also utilizes the QPE subroutine for its speed-up [3, 6]. QPEA has applications in quantum sampling [14, 15]. Furthermore, the QPE problem is relevant to clock synchronization, magnetometry, etc. [16–24]. Experimental implementations of the QPEA include those in Refs. [11–13, 25–28].

In realistic situations, the computational machines do not operate as we would like them to do ideally. The reasons behind the flaws might be some imperfections present in the building blocks or unrecognized or uncontrolled interactions of the devices with the environment. It is thus reasonable to explore the effects of noise on the performance of the quantum phase estimation process. QPE has been analyzed by considering various physically relevant noise models [29–42]. For example, the effects of white, bit flip, phase flip, and bit-phase flip noise on QPEA are discussed in [32, 34]. In optical interferometry, the fundamental limits to precision of phase estimation for light with definite photon number is discussed in [43], in the presence of photon loss. In absence of entanglement in the system, error in the estimated phase scales as the inverse square root of the photon number; while, taking advantage of entanglement, it can be improved to an inverse photon number scaling, known as the Heisenberg limit [44].

Using the Cramér-Rao bound [45] and the concept of Fisher information [46, 47], several studies have demonstrated that the expected precision can deviate from the Heisenberg limit in presence of noise [35, 37, 38].

In this paper, we study the effects of noise induced by “glassy disorder”, in the circuit components, on the quantum phase estimation algorithm. We assume that only the Hadamard gates are affected by such disorder. Three types of glassy disorders are considered: uniform (Haar-uniform with a circular cut-off), squeezed (Haar-uniform with an elliptical cut-off), and spherical normal (von Mises-Fisher). We find that the depreciation in probability, with increasing disorder degree, of correctly predicting the phase is related to the number of auxiliary qubits used in the algorithm. In the case of uniform disorder, when the noise is weak, the probability changes slowly with the degree of disorder. After crossing a threshold amount of disorder, a sudden change in probability is observed; that is, the rate of fall of the probability with increasing disorder, gets faster. Further increasing the disorder, a cut-off is encountered, after which the probability becomes almost constant. These thresholds and cut-off values depend on the number of auxiliary qubits. In particular, the number of participating auxiliary qubits has a log-log dependence on the disorder amount at which the concave to convex transition is noticed. The minimum probability of successful detection of phase, with a certain precision, exhibits the same feature. We see that larger the number of auxiliary qubits used, greater is the effect of disorder on the probabilities. We also observe that the squeezed disorder has more effect on the algorithm than the non-squeezed uniform disorder, for the same projected areas of the two disorders.

The rest of the paper is organized as follows. In Sec. II, we briefly review the quantum phase estimation algorithm. Sec. III consists of a description of the disorder that we impose, along with a short discussion on the three specific disorder distributions we consider. We proceed to our main results in Sec. IV, where we discuss the response of the algorithm to the various types of distributions. A conclusion is presented in Section V. Two appendices discuss the supplementary material.

II. PHASE ESTIMATION ALGORITHM

In this section, we will briefly recapitulate the quantum Fourier transform-based QPEA [9]. Suppose U is a unitary operator acting on an n -qubit Hilbert-space. One eigenvector of U is $|\psi\rangle$, and the corresponding eigenvalue is $e^{2\pi ip}$, where $p \in [0, 1)$. Thus we have

$$U |\psi\rangle = e^{2\pi ip} |\psi\rangle.$$

The aim of the algorithm is to estimate the phase, p , of the eigenvector, $|\psi\rangle$. A controlled- U gate, say $\Lambda_m(U)$, and auxiliary qubits are used to perform the algorithm. Let the number of available auxiliary qubits be m . $\Lambda_m(U)$ acts on the composite system consisting of $m + n$ qubits, where the first m are the auxiliary control qubits and the remaining n are the target qubits. We denote the basis of each of the single-qubit Hilbert-space as $\{|0\rangle, |1\rangle\}$. The operation of $\Lambda_m(U)$ is defined as

$$\Lambda_m(U) |k\rangle |\psi\rangle = |k\rangle (U^k |\psi\rangle) = e^{2\pi i k p} |k\rangle |\psi\rangle.$$

Here, k is the decimal number corresponding to the binary number representing the m -qubit auxiliary state. Thus, $k \in \{0, 1, \dots, 2^m - 1\}$.

To perform the algorithm, the state, $|\chi_0\rangle = |0\rangle^{\otimes m} |\psi\rangle$ is prepared initially. Next, Hadamard gates are acted upon the auxiliary qubits, transforming the initial state, $|\chi_0\rangle$, to $|\chi_1\rangle = \frac{1}{\sqrt{2^m}} \sum_{k=0}^{2^m-1} |k\rangle |\psi\rangle$. The information about p can be encoded in the m auxiliary qubits via a single application of the controlled- U gate. The controlled unitary transformation, $\Lambda_m(U)$, results in a phase kickback effect, that brings out the phase p in the following way:

$$|\chi_2\rangle = \Lambda_m(U) |\chi_1\rangle = \frac{1}{\sqrt{2^m}} \sum_{k=0}^{2^m-1} e^{2\pi i k p} |k\rangle |\psi\rangle. \quad (1)$$

At this point, it is possible to discard the state $|\psi\rangle$. $|\psi\rangle$ can be reused later if needed.

The quantum Fourier transformation is defined as follows

$$\text{QFT}_{2^m} |j\rangle = \frac{1}{\sqrt{2^m}} \sum_{k=0}^{2^m-1} e^{2\pi i j k / 2^m} |k\rangle.$$

Acting the $\text{QFT}_{2^m}^\dagger$, on the auxiliary qubits, the resulting state one gets is

$$|\zeta\rangle = \sum_{j=0}^{2^m-1} \left(\frac{1}{\sqrt{2^m}} \sum_{k=0}^{2^m-1} e^{2\pi i k (p-j/2^m)} \right) |j\rangle.$$

Finally, a projective measurement can be performed on the auxiliary states of $|\zeta\rangle$, in the computational basis, $\{|j\rangle\}_{j=0}^{2^m-1}$. The outcome corresponding to the output state $|j\rangle$, which is expected to represent the estimated phase, can be defined to be $\frac{j}{2^m}$. Then the probability of getting the outcome $\frac{j}{2^m}$ is

$$p_j = \left| \frac{1}{\sqrt{2^m}} \sum_{k=0}^{2^m-1} e^{2\pi i k (p-j/2^m)} \right|^2.$$

For the special case when $p = j/2^m$, p_j is exactly equal to 1, hence in that case the outcome can accurately estimate the phase, i.e. $p = \frac{j}{2^m}$. But in general $p = j/2^m + \delta$, where δ is a real number such that $|\delta| \leq 2^{-(m+1)}$, and j is an arbitrary integer satisfying $0 \leq j \leq 2^m - 1$. In that case, the probability of the outcome j is $p_j \geq \frac{4}{\pi^2} > 0.4$ [2]. Thus the minimum probability of successfully gathering information about the phase of the eigenvector, $|\psi\rangle$, with accuracy up to m binary points, is $p_{\min} = \frac{4}{\pi^2}$, that is when $\delta = 2^{-(m+1)}$. Thus it is straightforward that one can exponentially increase the accuracy of the obtained phase by increasing the number of the auxiliary qubits.

III. INCORPORATION OF DISORDER

The central focus of this work is to analyze how imperfections disturb the QPEA. The special class of disorders which we consider to be present in the algorithm are referred in the literature as “glassy” or “quenched” disorder. A system parameter is said to be quenched disordered when the equilibrium time of the disorder in the system is much larger than the typical observation time. This means that a particular realization of the disordered parameters do not change during the time of the observation. The values may change after a long time but that range of time is not in the domain of our interest.

To incorporate defects, we assume the Hadamard gates acting on the initial m auxiliary qubits’ states, $|0\rangle$, are affected by noise, and as a result, instead of transforming the state $|0\rangle$ ($|1\rangle$) to $|+\rangle = \frac{|0\rangle+|1\rangle}{\sqrt{2}}$ ($|-\rangle = \frac{|0\rangle-|1\rangle}{\sqrt{2}}$), the gate maps $|0\rangle$ ($|1\rangle$) to another state, say $|\xi(\theta, \phi)\rangle$ ($|\xi^\perp(\theta, \phi)\rangle$), on the surface of the Bloch sphere. Here, $|\xi^\perp(\theta, \phi)\rangle$ is a vector (unique up to phase) orthogonal to $|\xi(\theta, \phi)\rangle$, and (θ, ϕ) are spherical polar coordinates on the Bloch sphere. We denote such “noisy” Hadamard gates as $H(\theta, \phi)$ and define the operation of $H(\theta, \phi)$ on the single qubit states, $|0\rangle$ and $|1\rangle$, in the following way:

$$H(\theta, \phi) |0\rangle = |\xi(\theta, \phi)\rangle := \cos \frac{\theta}{2} |0\rangle + e^{i\phi} \sin \frac{\theta}{2} |1\rangle, \quad (2)$$

$$H(\theta, \phi) |1\rangle = |\xi^\perp(\theta, \phi)\rangle := \sin \frac{\theta}{2} |0\rangle - e^{i\phi} \cos \frac{\theta}{2} |1\rangle. \quad (3)$$

$\theta = \frac{\pi}{2}$ and $\phi = 0$ represents the mapping under the “noiseless” (i.e., the usual) Hadamard gate. In the disordered case, each of the pair of angles, (θ, ϕ) , defining the operation of the Hadamard gate on the auxiliary qubits, will be chosen from an appropriate distribution depending on the type of the disorder we impose. This can also be thought as of choosing the state $|\xi(\theta, \phi)\rangle$ or $|\xi^\perp(\theta, \phi)\rangle$ from the surface of the Bloch sphere. Generally, the zenith angle, θ , and the azimuthal angle, ϕ , being the spherical polar coordinates, belong in the ranges $[0, \pi]$ and $[0, 2\pi)$ respectively, but the ranges may get shortened in case of special disorders.

The quantity of interest, in our case, is the probability of obtaining correct output which can represent the phase accurately up to m binary places. We denote each of the zenith and azimuthal angles as θ_i and ϕ_i , which defines operation of each of the noisy Hadamard gates, $H_i(\theta_i, \phi_i)$, on the i th auxiliary qubit. Then after the measurement of the final state in the

computational basis $\{|j\rangle\}_{j=0}^{2^m-1}$, the probability of obtaining an output state $|j\rangle$ is

$$p'_j = \frac{1}{2^m} \prod_{i=1}^m \left[1 + \sin \theta_i \cos \left[2^i \pi \left(p - \frac{j}{2^m} \right) + \phi_i \right] \right]. \quad (4)$$

For detailed derivation, see Appendix VI.

The “quenched average” of a quantity is defined as the average of the quantity evaluated over the distributions of the disorders under discussion. Thus, here the quenched averaged probability can be obtained as

$$q_j = \int \cdots \int p'_j(m) \prod_{i=1}^m f(\theta_i, \phi_i) \sin \theta_i d\theta_i d\phi_i, \quad (5)$$

where $f(\theta_i, \phi_i)$ is the probability density function of the distributions that the disorders follow. Keeping in mind realistic scenarios, we assume each pair of the angles, (θ_i, ϕ_i) , follow same disorder distribution.

In the same manner, we can determine the minimum probability of obtaining the phase, accurate up to m binary points, in presence of disorder, as

$$p'_{min} = \frac{1}{2^m} \prod_{i=1}^m \left[1 + \sin \theta_i \cos \left[\frac{2^i \pi}{2^{m+1}} + \phi_i \right] \right].$$

The quenched averaged value of p'_{min} is denoted as q_{min} and defined as

$$q_{min} = \int \cdots \int p'_{min}(m) \prod_{i=1}^m f(\theta_i, \phi_i) \sin \theta_i d\theta_i d\phi_i.$$

In this work, we will consider three different types of disorder distributions followed by the angles (θ_i, ϕ_i) . The following subsections consists of discussion on these distributions.

For the sake of lucid descriptions given in the remaining part of the paper, we define three axes on the Bloch sphere, that are the line joining the eigenstates of the Pauli x or y or z matrix which we name as x or y or z axis, respectively. From now on, we use the notation $(1, \theta, \phi)$, to denote a point on the Bloch sphere that represents the state written in the RHS of Eq. (2).

A. Haar-uniform distribution

In the first type of disorder, we want the states, $\xi(\theta, \phi)$, to be uniformly and symmetrically distributed on the Bloch sphere, around $|+\rangle$. Since ideally the output of $H(\theta, \phi)|0\rangle$ should be $|+\rangle$, we constraint the distribution’s mean’s direction to be along the positive x -axis. For restricting the spread of the disorder, we define a circular boundary outside of which the probability density function is zero. To realize the boundary, imagine an infinite plane that is parallel to the y - z plane. That plane will cut the Bloch sphere, creating a circular boundary on the surface of the sphere. We will randomly select only those points which belongs on the positive x -direction of the plane. Let d be the angle, that $|+\rangle$ state and an arbitrary

state on the circular boundary make at the center of the Bloch sphere. This angle, d , can parametrize the degree or strength of the disorder. As the amount of disorder increases, the value of d becomes larger whereas $d = 0$ represents the noiseless case.

To model the situation in MatLab, we consider a circle on the surface of the sphere, around the z -axis. The circle is parallel to the x - y plane and have the same area as the boundary of the distribution within which we want to generate the points. We Haar-uniformly select (θ, ϕ) such that the corresponding point, $(1, \theta, \phi)$, fall on that surface which is situated on the positive z -direction of the circle. Then we rotate each point, around the y -axis, to turn it into a distribution around the x -axis.

B. Squeezed distribution

In the next case, the same distribution is considered as discussed in the previous section, with the only difference that this distribution is not symmetric about the mean, $|+\rangle$, i.e. the boundary here is not restrained to be circular. We are free to squeeze the circular boundary along y or z axis to get a curved elliptical surface on the Bloch sphere. To properly visualize this squeezed boundary, we consider an ellipse on the y - z plane. a and b denote the semi-axes lengths of the ellipse along y and z -axis, respectively. $a = b = 1$ represents the great circle on the y - z plane. We take the ellipse’s projection on the sphere. This projection is the new boundary of the Haar-uniformly generated points, $(1, \theta, \phi)$. We name the distribution of such points as “squeezed” distribution. Since the area of the ellipse, say D , can characterize the spreading of the distribution, D is considered as a measure of the disorder. The ratio $r = a/b$ denotes the degree of squeezing. D can be expressed, in terms of the semi-axes (a and b) and the ratio (r), as $D = \pi ab = \pi r b^2$. Since $a, b \leq 1$, $D \leq \pi$. Given an area D , the corresponding range of allowed values of r is obtained as follows:

- (i) If $r \geq 1$, $a_{max} = 1$ and $b_{min} = D/\pi$; $\therefore r_{max} = a_{max}/b_{min} = \pi/D$;
- (ii) If $r \leq 1$, $b_{max} = 1$ and $a_{min} = D/\pi$; $\therefore r_{min} = a_{min}/b_{max} = D/\pi$.

Here, $a_{max/min}$ and $b_{max/min}$ denote the maximum/minimum possible value of a and b respectively. Hence the range of r is $\left[\frac{D}{\pi}, \frac{\pi}{D}\right]$. $r = 1$ is the special distribution which was discussed in Sec III A. The angle d , defined for $r = 1$ case, is related to D as $d = \sin^{-1} \sqrt{D/\pi}$.

To have a clear understanding of the distribution, we depict the distribution in the left panel of Fig. 1, for two values of r , viz. $r = 2$ and $r = 0.5$. It can be observed that for $r > 1$, the circle is squeezed towards y axis, while it is squeezed towards z axis for $r < 1$.

C. von Mises-Fisher distribution

Lastly, we want to explore the impact of disorder following a “spherical normal”, precisely, the von Mises-Fisher dis-

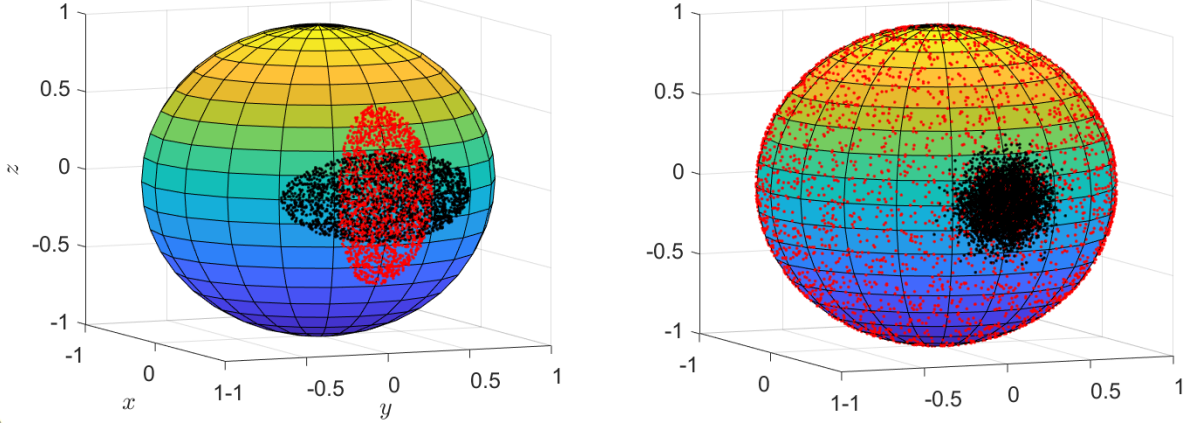


FIG. 1: Illustration of squeezed and von Mises-Fisher distributions on the surface of a unit sphere. In the left panel, we present the squeezed distribution, whereas in the right, the von Mises-Fisher distribution is exhibited. The quantities describing the nature of the former distribution are taken to be $D = 0.5244$, and $r = 2$ (black points) and 0.5 (red points). When $r > 1$ ($r < 1$) the distribution becomes extended along y (z) axis. The mean of the von Mises-Fisher distribution is specified to be along x direction. The values of the concentration parameter, κ , characterizing the distribution, is taken to be $\kappa = 70$ (black points) and $\kappa = 0$ (red points). Larger the value of κ , smaller is the corresponding spread of the distribution. All quantities used are dimensionless.

tribution, on QPEA. The von Mises-Fisher distribution is an analogue of the usual normal distribution on the surface of a $(P - 1)$ -dimensional unit sphere in \mathbb{R}^P [48]. The probability density function of a random point, following the von Mises-Fisher distribution, on a $(P - 1)$ -dimensional unit sphere situated at the origin, is given by

$$f_P(\mathbf{x}; \mu, \kappa) = C_P(\kappa) \exp(\kappa \mu^T \mathbf{x}),$$

where \mathbf{x} represents coordinate of the point. The parameters μ and κ denote the direction of mean and the concentration of points on the sphere, respectively, satisfying $\kappa \geq 0$ and $\|\mu\| = 1$. The normalization constant $C_P(\kappa)$ is equal to $\frac{\kappa^{P/2-1}}{(2\pi)^{P/2} I_{P/2-1}(\kappa)}$ with $I_{P/2-1}(\kappa)$ being the modified Bessel function of first kind at order $(P/2 - 1)$. The distribution is unimodal for $\kappa > 0$, and is uniform on the surface of the sphere, for $\kappa = 0$.

We want to generate points, $(1, \theta, \phi)$, on the Bloch sphere situated on a 3-dimensional space. Thus the distribution of our interest, i.e the von Mises-Fisher distribution for $P = 3$, is given by

$$f_3(\mathbf{x}; \mu, \kappa) = \frac{\kappa}{4\pi \sinh \kappa} \exp(\kappa \mu^T \mathbf{x}),$$

where $\mathbf{x} \equiv (\sin \theta \cos \phi, \sin \theta \sin \phi, \cos \theta)$. We take the direction of the mean axis to be $\mu = (1, \pi/2, 0)$. Since the concentration of the distributed points increase with κ , the measure of the disorder is defined to be $1/\kappa$. The generation of points are discussed thoroughly in Appendix VII.

We randomly choose points from the von Mises-Fisher distribution, for $\kappa = 0$ and $\kappa = 70$. The mean direction of these points are restricted to be along x -axis. These points are plotted on a surface of a unit sphere in Fig. 1. It is visible that the points corresponding to $\kappa = 0$ are uniformly distributed over the entire sphere whereas the the points corresponding to $\kappa = 70$, is symmetrically concentrated around x -axis.

IV. BEHAVIOR OF ALGORITHM IN RESPONSE TO DISORDER

In this section, we consider each of the three types of disorders separately, and explore the impact of the disorder on the QPE process. To realize this, we determine the quenched averaged probability, q_j , and examine its nature with the strength of the corresponding disorder.

Before going into the details, let us first discuss the numerical method for derivation of the quenched averaged probability. Depending on the parameter, defining the degree of the disorder, we independently select m pairs of angles (θ_i, ϕ_i) within the allowed range and evaluate p'_j using Eq. (4). This process is repeated multiple times until we get a bunch of p'_j s. We take the average of these p'_j s to obtain the quenched averaged probability, q_j . To check the convergence, we again determine the q_j for a larger set of p'_j s, and compare its value with the previous one. Finally, only those values of q_j s are noted which have converged up to 4th decimal place. This is valid since the way we generate points on the sphere satisfies $\int \int f(\theta, \phi) d\theta d\phi = 1$ within the range of the distribution.

A. Uniform disorder

In this part, we will determine the significance of uniform disorder on QPEA. In precise, we will consider noisy Hadamard gate whose output corresponding to the input $|0\rangle$, instead of being $|+\rangle$, is $\xi(\theta, \phi)$, where the angles (θ, ϕ) are such that the points $(1, \theta, \phi)$, are Haar uniformly distributed on the surface of the Bloch sphere. As we have mentioned previously, the amount of disorder will be quantified using the angle d . In the following paragraph (Sec. IV A 1), we will con-

sider two specific values of d and determine corresponding q_j . In the next paragraph (Sec. IV A 2), the noisy QPEA will be explored for a broader set of values of d .

1. Two special cases

We are going to discuss two types of situations separately, one is when the points, $(1, \theta, \phi)$, are distributed over the whole sphere, i.e. $d = \pi$, and the other is when $d = \pi/2$, i.e. the points are distributed over half of the sphere.

For $m = 1$, j of Eq. (4) can take only two distinct values, viz 0 and 1. Thus, we can evaluate the phase up to only one binary point, i.e. the phase will be known to be either $p = 0$ or $p = 0.5$. In case of disorder over the whole sphere, the corresponding quenched average probabilities are $q_0 = q_1 = 0.5$, for $m = 1$.

Similarly, for $m = 2$, the phase can be estimated up to two binary points, i.e. $p = 0, 0.25, 0.5$, or 0.75 , and the corresponding values of j are 0, 1, 2, and 3 respectively. In this case, $q_j = 0.25$, for all $j \in \{0, 1, 2, 3\}$.

For arbitrary number of auxiliary qubits, say m , the value of the quenched averaged probability is $q_j = 1/2^m$, for $j = \{0, 1, \dots, 2^m - 1\}$. We see, in case of $d = \pi$, q_j is independent of the error $\delta = p - \frac{j}{2^m}$, that means whatever be the phase, all the outcomes are equally probable. Thus, the QPEA, in presence of uniform disorder over the complete sphere, is not trustworthy.

In case of disorder over half of the sphere, the quenched averaged probability of a certain outcome $\frac{j}{2^m}$, for arbitrary number of auxiliary qubits, m , is given by

$$q_j = \frac{1}{2^{2m}} \prod_{i=1}^m \left[2 + \cos 2^i \pi \left(p - \frac{j}{2^m} \right) \right],$$

where $j = \{0, 1, \dots, 2^m - 1\}$. Let the actual phase be $p = \frac{j}{2^m} + \delta$, where $\delta \leq 2^{-(m+1)}$, then for example, if we take $m = 5$ and $\delta = 1/2^{10}$, q_j is approximately equal to 0.2368 which matches with the numerical result in Fig. 2 for $d = \pi/2$, i.e. disorder over the right-half sphere. The results reported in this paragraph (Sec. IV A 1) are obtained using analytical calculations.

2. Effect of uniform disorder having arbitrary strength

Let us proceed to the more general case, where the distribution of the disorder is still Haar-uniform but the amount of disorder, d , is varied more flexibly. The parameter, d , fixes the range of the distributed angles, (θ, ϕ) . By selecting Haar-uniform points within this range, and following the numerical process mentioned at the beginning of IV, we find the quenched averaged probability, q_j for different values of d . In the computation of q_j , we choose δ according to the following table:

m	5	15	25	35	45	175
$\log_2 \delta$	-10	-20	-30	-40	-50	-180

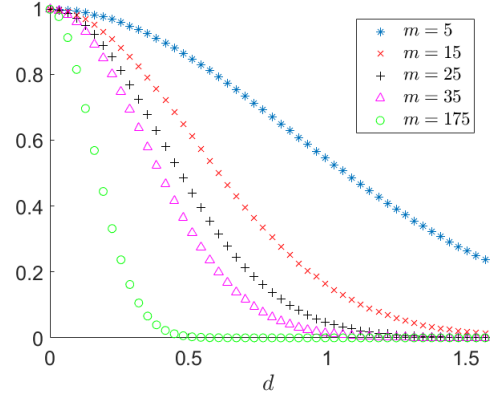


FIG. 2: Quenched averaged probability in presence of uniform disorder within Hadamard transformation. We show the variation of q_j with respect to the degree of disorder, d , for different number of used auxiliary qubits, m . The curves corresponding to various values of m are demonstrated using different colors and point type, as described in the legend. The horizontal axis represents d in the unit of radians, and is dimensionless. The corresponding quenched averaged probabilities are plotted along the dimensionless vertical axis.

We plot the results in Fig. 2. The figure shows the dependence of q_j on d , for different number of auxiliary qubits, m . It can be observed from the figure that when d is small, q_j decreases slowly with increasing d . When the disorder is increased further, suddenly the probability starts to decrease drastically. The threshold value of d , at which the change from the slow decrease to fast decrease takes place, depends on m . Higher the value of m , smaller is the corresponding threshold d . Again, at high disorder range the probability becomes almost constant. This saturated value, say p_{sat} , also depends on m . For sufficiently large m , e.g. $m \geq 15$, $p_{sat} \sim 0$ at $d = \pi/2$ i.e. the special case when the output states, $\xi(\theta, \phi)$, are distributed over the half-sphere.

For each value of m , the corresponding curve, in Fig. 2, changes from concave to convex at a particular d , which is more prominent for higher values of m . To determine the inflection point, d_c , we present the derivatives of the quenched averaged probabilities with respect to d in Fig. 3 (a), for different values of m . The minimum of each of the curves in Fig. 3 (a), indicates the point, d_c . Certainly d_c depends on m . For higher value of m , d_c gets closer to zero. We can define two regions: “weak” disorder, when the amount of disorder, d , is much smaller than d_c , and “high” disorder, when d is significantly larger than d_c . In Fig. 3 (b), we plot d_c versus m . It can be realized from the figure that there is a log-log dependence between d_c and m . We can fit the curve using the following function:

$$\log_e(d_c - \alpha) = \log_e \beta + \gamma \log_e m, \quad (6)$$

where the fitting parameters are given by $\alpha = -0.11 \pm 0.18$, $\beta = 1.7 \pm 0.16$, and $\gamma = -0.38 \pm 0.14$. The curve is fitted using least square method. The least square error obtained in

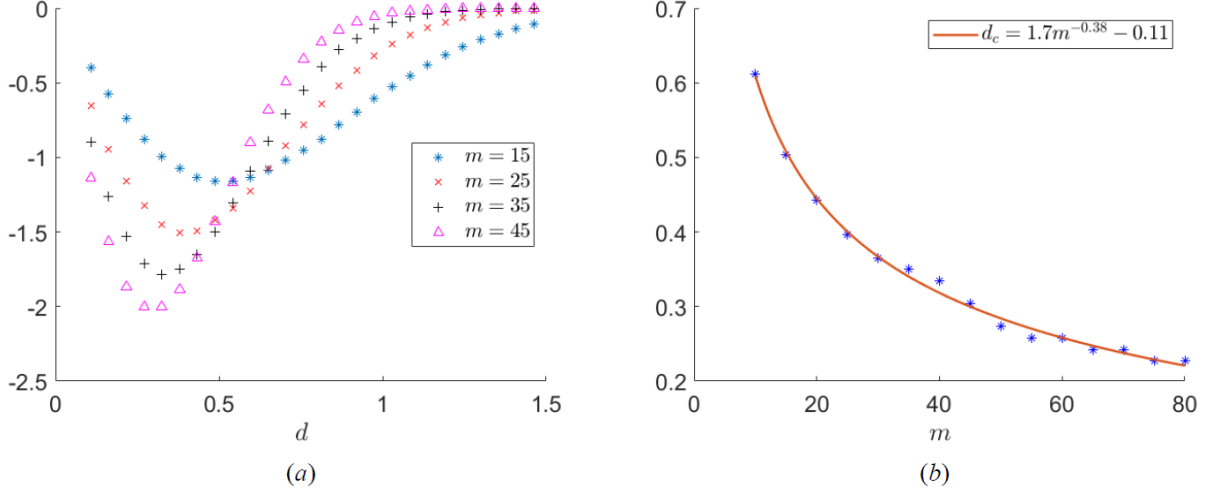


FIG. 3: How does the effect of disorder depends on the number of used auxiliary qubits? (a) All the considerations are the same as in Fig. 2, except that the vertical axis here represents the derivatives of quenched probabilities with respect to d . (b) The vertical axis represents d_c , the minima of the curves presented in Fig. 3 (a). This is the point where the corresponding curve in Fig. 2 changes concavity. The horizontal axis represents m . Both the axes are dimensionless but the vertical axis has unit of radians. The blue points represents the numerically found data whereas the Eq. (6) is plotted using red line, which represents the fitted curve.

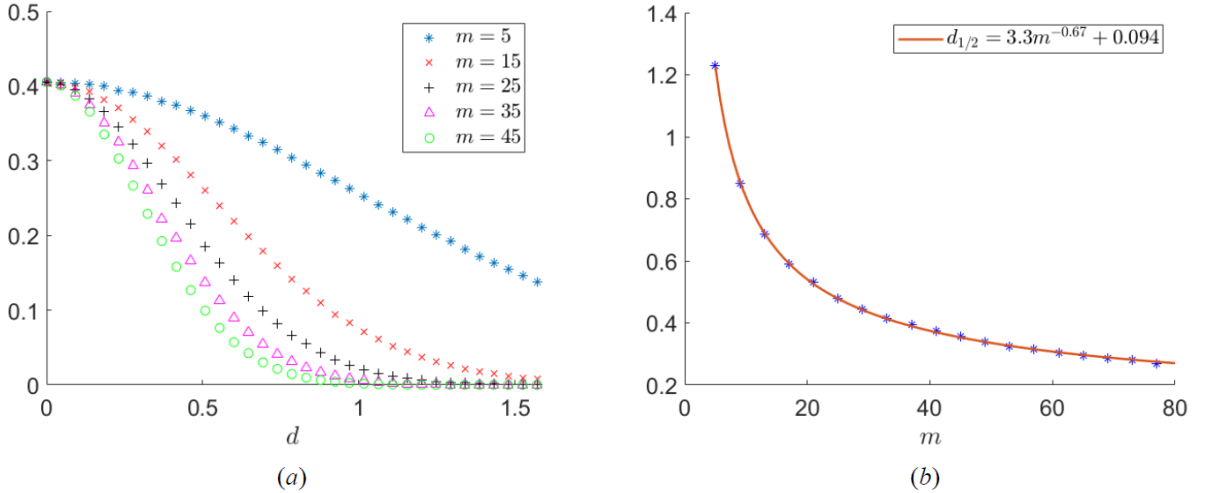


FIG. 4: Behavior of the quenched averaged minimum probability of correctly obtaining the phase with a predefined precision. (a) The considerations are the same as in Fig. 2, except that the vertical axis denotes q_{min} . (b) The vertical axis denotes $d_{1/2}$, the disorder at which the quenched averaged probability, q_{min} reduces to half of the value of p_{min} , that is the probability in the noiseless situation. The horizontal axis represents m . The data points are plotted using blue color points. These points are then fitted with the curve given in Eq. (7). The fitted curve is shown in the figure using a red line.

this fitting is 8.0×10^{-4} . Numbers, that are written after \pm sign, denote the 95% confidence interval of the corresponding parameter's value.

As stated in section II, and discussed in Ref. [2], $p_{min} \sim 0.4$ for large m , i.e $m \geq 5$. Fig. 4 (a) represents how quenched averaged value of p'_{min} , i.e q_{min} varies with the amount of disorder, d . In the noiseless situation, i.e. for $d = 0$, q_{min} take val-

ues close to 0.4 for all values of m , and then start to decrease with increasing d . This degradation becomes faster for greater values of m . The pattern of the curves shown in Fig. 4 (a) are similar to the curves shown in Fig. 2. We see for large number of auxiliary qubits, the noise from each Hadamard gate some what sums up, affecting the qubits too much and thus the collective impact of the noise dominates over the benefit

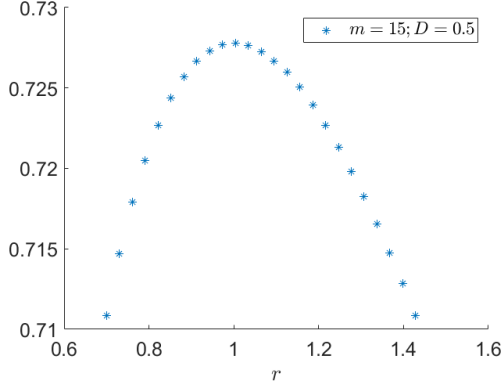


FIG. 5: Response of probability of getting exact outcome, to squeezed circular disorder. We plot q_j along the horizontal axis, with respect to the degree of squeezing, r , which is represented along the vertical axis. The plot corresponds to the case when the area of the elliptical projection of the distributed point on the y - z plane, is $D = 0.50$. When $r = 1$ the boundary of distributed points attains the shape of a circle that can be described using the parameter value $d = \sin^{-1} \sqrt{0.5/\pi}$. $m = 15$ auxiliary qubits are considered to be used in the algorithm. Both axes are dimensionless.

from large m .

Now we compute the disorder at which the quenched averaged probability, q_{min} , reduces to half of its original value, i.e the value in the noiseless case, p_{min} . We denote this disorder by $d_{1/2}$. The dependence of $d_{1/2}$ on m is plotted in Fig. 4 (b). Intuitively, this gives an impression on how fast the probability fall with increasing auxiliary qubits. This curve also has a log-log dependence. The following function is used to fit the curve:

$$\log_e(d_{1/2} - \alpha) = \log_e \beta + \gamma \log_e(m). \quad (7)$$

where $\alpha = 0.094 \pm 0.014$, $\beta = 3.3 \pm 0.083$, and $\gamma = -0.67 \pm 0.020$. The least-square error in the fitting is found to be 3.6×10^{-5} .

B. Squeezed disorder

Let us now discuss the impact of the disorder, following squeezed distribution, on the probability of obtaining correct outcome. p'_j is plotted as a function of r , in Fig. 5, for a fixed number of auxiliary qubits, $m = 15$, and $D = 0.5$. It can be noticed from the figure that the value of the quenched averaged probability is same for squeezing strength r and $1/r$. Thus, it is apparent that the probability is symmetric about the direction of squeezing.

C. Spherical normal disorder

We now consider the case when the disorder follows the von Mises-Fisher distribution. Fig. 6 shows the variation of

the quenched averaged probability with respect to $1/\kappa$. As described in Sec. III C, κ is a measure of the disorder present in the Hadamard gate. Hence, smaller the value of κ , larger is the effect of disorder. As a result, the quenched averaged probability takes value near unity, for all m , in noiseless situation and start decreasing monotonically with increasing $1/\kappa$. The von Mises-Fisher distribution, also, seems to be affecting more, when the number of auxiliary qubits is large.

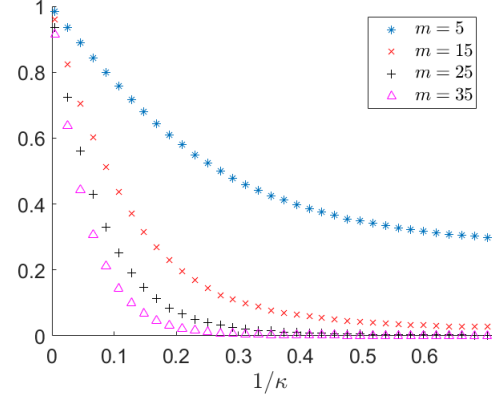


FIG. 6: Probability of getting appropriate outcome in presence of spherical normal disorder. We present the values of q_j with respect to $1/\kappa$, for different values of m using different point type, as mentioned in the legend. The axes are dimensionless.

V. CONCLUSION

The quantum phase estimation algorithm lies at the heart of several applications in quantum information and computation. In realistic scenarios, both environmental noise and noise due to imperfections within the circuit affect the performance of the algorithm in estimating the correct phase value up to a desired precision. We investigated the effects of “glassy disorder” originating from faulty Hadamard gates used in the quantum phase estimation circuit.

We studied three disorder distributions, viz. Haar-uniform with a finite circular cut-off, Haar-uniform with an elliptical (squeezed) cut-off, and von Mises-Fisher disorder. We derived the quenched averaged probability of measuring the correct phase value, and its dependence on the degree of disorder. We observed that the depreciation of the success probability from its ideal value depends on the number of auxiliary states used in the algorithm. We saw that the quenched average probability changes from concave to a convex function of disorder strength, for uniform distributions. In the case of uniform disorder, we also estimated a log-log dependence between the inflection point and the number of performing auxiliary qubits. Our work is potentially a step towards creating a dictionary for an experimenter of her expectation of the capability of the quantum phase estimation process in a realistic, noisy, scenario.

Acknowledgment: S.M. acknowledges support from the KVPY program. We acknowledge partial support from the Department of Science and Technology, Government of India through the QuEST grant (grant no. DST/ICPS/QUST/Theme-3/2019/120).

VI. APPENDIX-A

In the phase estimation algorithm the initial state of the auxiliary qubits are considered to be $|\zeta_0\rangle = |0\rangle^{\otimes m}$. After the application of noisy H -gates, the state of the system of m auxiliary qubits becomes

$$\begin{aligned} |\zeta'_1\rangle &= H_m |0\rangle \dots H_1 |0\rangle \\ &= \left(\cos \frac{\theta_m}{2} |0\rangle + e^{i\phi_m} \sin \frac{\theta_m}{2} |1\rangle \right) \otimes \\ &\quad \dots \otimes \left(\cos \frac{\theta_1}{2} |0\rangle + e^{i\phi_1} \sin \frac{\theta_1}{2} |1\rangle \right), \end{aligned}$$

where θ_i and ϕ_i describe the independent local disorder, present in the noisy Hadamard gate H_i . Operation of the controlled-U gate on $|\zeta'_1\rangle$, produces the state

$$\begin{aligned} |\zeta'_2\rangle &= \Lambda_m(U) |\zeta'_1\rangle = \left(\cos \frac{\theta_m}{2} |0\rangle + e^{2\pi i p} e^{i\phi_m} \sin \frac{\theta_m}{2} |1\rangle \right) \otimes \\ &\quad \dots \otimes \left(\cos \frac{\theta_1}{2} |0\rangle + e^{2\pi i p} e^{i\phi_1} \sin \frac{\theta_1}{2} |1\rangle \right). \end{aligned}$$

This can be written in terms of $|k\rangle$, where k denote the decimal representation of the binary number depicting the m -qubit auxiliary state, in the following way

$$\begin{aligned} |\zeta'_2\rangle &= \cos \frac{\theta_m}{2} \dots \cos \frac{\theta_2}{2} \cos \frac{\theta_1}{2} |0\rangle \\ &\quad + e^{2\pi i p + i\phi_1} \cos \frac{\theta_m}{2} \dots \cos \frac{\theta_2}{2} \sin \frac{\theta_1}{2} |1\rangle \\ &\quad + \dots + e^{(2^m - 1)2\pi i p + i(\phi_1 + \dots + \phi_m)} \sin \frac{\theta_m}{2} \dots \sin \frac{\theta_1}{2} |2^m - 1\rangle. \end{aligned} \quad (8)$$

$|\zeta'_2\rangle$, given in (8), can be expressed as $\sum_{k=0}^{2^m-1} y_k |k\rangle$. The application of $\text{QFT}_{2^m}^\dagger$ on $\sum_{k=0}^{2^m-1} y_k |k\rangle$ will produce the state $|\zeta'_3\rangle = \text{QFT}_{2^m}^\dagger |\zeta'_2\rangle = \text{QFT}_{2^m}^\dagger \sum_{k=0}^{2^m-1} y_k |k\rangle = \sum_{j=0}^{2^m-1} x_j |j\rangle$, where the coefficients, x_j , are given by

$$\begin{aligned} x_j &= \frac{1}{\sqrt{2^m}} \sum_{k=0}^{2^m-1} y_k e^{-\frac{2\pi i j k}{2^m}} \\ &= \frac{1}{\sqrt{2^m}} \prod_{l=1}^m \left[\cos \frac{\theta_l}{2} + e^{2\pi i (p - \frac{j}{2^m}) + i\phi_l} \sin \frac{\theta_l}{2} \right], \end{aligned}$$

On measurement of the auxiliary states in the computational basis $\{|j\rangle\}_{j=0}^{2^m-1}$, we obtain the state $|j\rangle$ with probability

$$p_j = |x_j|^2 = \frac{1}{2^m} \prod_{l=1}^m \left[1 + \sin \theta_l \cos \left[2^l \pi \left(p - \frac{j}{2^m} \right) + \phi_l \right] \right].$$

VII. APPENDIX-B

We begin by generating a distribution of points around the z -axis on Bloch sphere. Hence $\boldsymbol{\mu} = (0, 0, 1)^T$ and $\mathbf{x} = (\sin \theta \cos \phi, \sin \theta \sin \phi, \cos \theta)^T$ gives $\boldsymbol{\mu}^T \mathbf{x} = \cos \theta$. Since the dimension of Bloch sphere is 3, we take $p = 3$. The normalization constant here is

$$C_3(\kappa) = \frac{\sqrt{\kappa}}{(\sqrt{2\pi})^3 I_{1/2}(\kappa)} = \frac{\kappa}{4\pi \sinh \kappa},$$

and $I_{1/2} = \sqrt{\frac{2}{\pi\kappa}} \sinh \kappa$. Thus the required probability density function is

$$f_3(\theta) = \frac{\kappa}{4\pi \sinh \kappa} \exp(\kappa \cos \theta).$$

Since we want to generate points that follow the above distribution, we first compute the cumulative distribution function,

$$F(\theta) = \int_0^\theta 2\pi f_3(\theta') \sin \theta' d\theta' = \frac{e^\kappa - e^{\kappa \cos \theta}}{2 \sinh \kappa}.$$

The range $\theta \in [0, \pi]$ confirms $F(\theta) \in [0, 1]$. For a certain constant A , if $F(\theta) = A$, the inverse is given by

$$\theta = \cos^{-1} \left[\frac{1}{\kappa} \ln(e^\kappa - 2A \sinh \kappa) \right] = F^{-1}(A).$$

Choosing A from a uniform distribution within the range $[0, 1]$, we can generate θ that follows von Mises-Fisher distribution. All that remains is to select ϕ randomly from the uniform distribution over the range $[0, 2\pi]$ to create a distribution of points around the z -axis. Then we rotate each points by operating the matrix

$$A = \begin{pmatrix} 0 & 0 & 1 \\ 0 & 1 & 0 \\ -1 & 0 & 0 \end{pmatrix}$$

on $(\sin \theta \cos \phi, \sin \theta \sin \phi, \cos \theta)^T$, and turn it into a distribution of points around the x -axis.

-
- [1] R. Cleve, A. Ekert, C. Macchiavello, and M. Mosca, *Quantum algorithms revisited*, Proc. R. Soc. Lond. A **454**, 339 (1998).
 [2] J. Watrous, *Introduction to Quantum Computing*, Lecture 9, Page 57 (2005), <https://cs.uwaterloo.ca/~watrous/QC-notes/QC->

notes.pdf.

- [3] M. A. Nielsen and I. L. Chuang, *Quantum Computation and Quantum Information* (Cambridge University Press, New York, 2010).

- [4] D. Deutsch, *Quantum theory, the Church–Turing principle and the universal quantum computer*, Proc. R. Soc. London A **400**, 97 (1985).
- [5] D. Deutsch and R. Jozsa, *Rapid solution of problems by quantum computation*, Proc. R. Soc. Lond. A **439**, 553 (1992).
- [6] P. W. Shor, *Polynomial-time algorithms for prime factorization and discrete logarithms on a quantum computer*, SIAM J. Comput. **26**, 1484 (1996).
- [7] L. K. Grover, *A fast quantum mechanical algorithm for database search*, Proceedings of the 28th Annual ACM Symposium on the Theory of Computing (STOC 1996), 212 (1996).
- [8] A. Y. Kitaev, *Quantum measurements and the Abelian Stabilizer Problem*, Electron. Colloq. Comput. Complex. **3** (1996); arXiv:quant-ph/9511026.
- [9] D. S. Abrams and S. Lloyd, *Quantum Algorithm Providing Exponential Speed Increase for Finding Eigenvalues and Eigenvectors*, Phys. Rev. Lett. **83**, 5162 (1999).
- [10] A. Yu. Kitaev, A. H. Shen, and M. N. Vyalyi, *Classical and Quantum Computation* (American Mathematical Society, Rhode Island, 2002).
- [11] B. P. Lanyon, J. D. Whitfield, G. G. Gillett, M. E. Goggin, M. P. Almeida, I. Kassal, J. D. Biamonte, M. Mohseni, B. J. Powell, M. Barbieri, A. Aspuru-Guzik, and A. G. White *Towards quantum chemistry on a quantum computer*, Nat. Chem. **2**, 106 (2010).
- [12] J. Du, N. Xu, X. Peng, P. Wang, S. Wu, and D. Lu, *NMR Implementation of a Molecular Hydrogen Quantum Simulation with Adiabatic State Preparation*, Phys. Rev. Lett. **104**, 030502 (2010).
- [13] P. J. J. O’Malley et al., *Scalable Quantum Simulation of Molecular Energies*, Phys. Rev. X **6**, 031007 (2016).
- [14] K. Temme, T. J. Osborne, K.G. Vollbrecht, D. Poulin, and F. Verstraete, *Quantum Metropolis Sampling*, Nature **471**, 87 (2011).
- [15] M. Ozols, M. Roetteler, and J. Roland, *Quantum rejection sampling*, in Proceedings of the 3rd Innovations in Theoretical Computer Science Conference on - ITCS 12, 290 (2012).
- [16] Y. C. Eldar and G. D. Forney, *On quantum detection and the square-root measurement*, IEEE Trans. Inf. Theory **47**, 858 (2001).
- [17] Y. C. Eldar and A. V. Oppenheim, *Quantum signal processing*, IEEE Signal Process. Mag. **19**, 12 (2002).
- [18] T. Rudolph, L. Grover, *Quantum communication complexity of establishing a shared reference frame*, Phys. Rev. Lett. **91**, 217905 (2003).
- [19] M. de Burgh, S. D. Bartlett, *Quantum methods for clock synchronization: Beating the standard quantum limit without entanglement*, Phys. Rev. A **72**, 042301 (2005).
- [20] Y. Deville, *ICA-based and second-order separability of nonlinear models involving reference signals: general properties and application to quantum bits*, Signal Process. **92**, 1785 (2012).
- [21] E. M. Kessler, P. Kómár, M. Bishof, L. Jiang, A. S. Sørensen, and J. Ye, M. D. Lukin, *A quantum network of clocks*, Nat. Phys. **10**, 582 (2014).
- [22] J. Zhang, K. Li, S. Chong, and H. Wang, *Efficient reconstruction of density matrices for high dimensional quantum state tomography*, Signal Process. **139**, 136 (2017).
- [23] Y. Deville and A. Deville, *Blind quantum source separation: quantum-processing qubit upcoupling systems based on disentanglement*, Digit. Signal Process. **67**, 30 (2017).
- [24] J. Zhang, S. Cong, Q. Ling, K. Li, *An efficient and fast quantum state estimator with sparse disturbance*, IEEE Trans. Cybern. **49**, 2546 (2019).
- [25] E. Martin-Lopez, A. Laing, T. Lawson, R. Alvarez, X. Q. Zhou, and J. L. O’Brien, *Experimental realization of Shor’s quantum factoring algorithm using qubit recycling*, Nat. Photonics **6**, 773 (2012).
- [26] T. Monz, D. Nigg, E. A. Martinez, M. F. Brandl, P. Schindler, R. Rines, S. X. Wang, and I. L. Chuang, R. Blatt, *Realization of a scalable Shor algorithm*, Science **351**, 1068 (2016).
- [27] S. Paesani, A. A. Gentile, R. Santagati, J. Wang, N. Wiebe, D. P. Tew, J. L. O’Brien, and M. G. Thompson, *Experimental Bayesian Quantum Phase Estimation on a Silicon Photonic Chip*, Phys. Rev. Lett. **118**, 100503 (2017).
- [28] B. P. Lanyon, T. J. Weinhold, N. K. Langford, M. Barbieri, D. F. V. James, A. Gilchrist, and A. G. White, *Experimental Demonstration of a Compiled Version of Shor’s Algorithm with Quantum Entanglement*, Phys. Rev. Lett. **99**, 250505 (2007).
- [29] I. García-Mata and D. L. Shepelyansky, *Quantum phase estimation algorithm in presence of static imperfections*, Eur. Phys. J. D **47**, 151 (2008).
- [30] B. Teklu, M. G. Genoni, S. Olivares, and M. G. A. Paris, *Phase estimation in the presence of phase diffusion: the qubit case*, Phys. Scr. **2010**, 014062 (2010).
- [31] J. M. Chappell, M. A. Lohe, L. von Smekal, A. Iqbal, and D. Abbott, *A precise error bound for quantum phase estimation*, PLoS ONE **6**, 1 (2011).
- [32] E. Tesio, S. Olivares, and M. G. A. Paris, *Optimized Qubit Phase Estimation in Noisy Quantum Channels*, International Journal of Quantum Information **9**, 379 (2011).
- [33] M. G. Genoni, S. Olivares, and M. G. A. Paris, *Optical Phase Estimation in the Presence of Phase Diffusion*, Phys. Rev. Lett. **106**, 153603 (2011).
- [34] Y. Yao, L. Z. Ge, X. Xiao, X. Wang, and C. P. Sun, *Multiple phase estimation for arbitrary pure states under white noise*, Phys. Rev. A **90**, 062113 (2014).
- [35] J. D. Yue, Y. R. Zhang, and H. Fan, *Quantum-enhanced metrology for multiple phase estimation with noise*, Sci. Rep. **4**, 5933 (2014).
- [36] T. Kaftal and R. Demkowicz-Dobrzański, *Usefulness of an enhanced Kitaev phase-estimation algorithm in quantum metrology and computation*, Phys. Rev. A **90**, 062313 (2014).
- [37] F. Chapeau-Blondeau, *Optimized probing states for qubit phase estimation with general quantum noise*, Phys. Rev. A **91**, 052310 (2015).
- [38] F. Chapeau-Blondeau, *Entanglement-assisted quantum parameter estimation from a noisy qubit pair: A Fisher information analysis*, Phys. Lett. A **381**, 1369 (2017).
- [39] T. E. O’Brien, B. Tarasinski, and B. M. Terhal, *Quantum phase estimation of multiple eigenvalues for small-scale (noisy) experiments*, New J. Phys. **21**, 023022 (2019).
- [40] L. Pezzè and A. Smerzi, *Quantum Phase Estimation Algorithm with Gaussian Spin States*, arXiv:2010.04001.
- [41] F. Chapeau-Blondeau and E. Belin, *Fourier-transform quantum phase estimation with quantum phase noise*, Signal. Process. **170**, 107441 (2020).
- [42] N. F. Costa, Y. Omar, A. Sultanov, and G. S. Paraoanu *Benchmarking Machine Learning Algorithms for Adaptive Quantum Phase Estimation with Noisy Intermediate-Scale Quantum Sensors*, EPJ Quantum Technol. **8**, 16 (2021).
- [43] U. Dörner, R. Demkowicz-Dobrzański, B. J. Smith, J. S. Lundeen, W. Wasilewski, K. Banaszek, and I. A. Walmsley, *Optimal Quantum Phase Estimation*, Phys. Rev. Lett. **102**, 040403 (2009).
- [44] A. S. Lane, S. L. Braunstein, and C. M. Caves, *Maximum-likelihood statistics of multiple quantum phase measurements*, Phys. Rev. A **47**, 1667 (1993).
- [45] H. Cramér, *Mathematical methods of statistics* (Princeton Uni-

- versity, Princeton, 1946).
- [46] C. W. Helstrom, *Quantum detection and estimation theory* (Academic Press, New York, 1976).
- [47] A. S. Holevo, *Probabilistic and statistical aspects of quantum theory* (North-Holland, Amsterdam, 1982).
- [48] R. M. Clark and B. J. Morrison, *A normal approximation to the Fisher distribution*, Geophys. J. R. Astr. Soc. **13**, 271 (1983).